Proceedings of the ASME International Manufacturing Science and Engineering Conference 2009
MSEC09
October 4-7, 2009, West Lafayette, Indiana, USA

MSEC2009-84319

THE EFFECTS OF INTEGRATION TIME AND SIZE-OF-SOURCE ON THE TEMPERATURE MEASUREMENT OF SEGMENTED CHIP FORMATION USING INFRARED THERMOGRAPHY

Jarred C. Heigel
National Institute of Standards and Technology[1]
Gaithersburg, MD, USA
jarred.heigel@nist.gov

Eric P. Whitenton
National Institute of Standards and Technology
Gaithersburg, MD, USA
eric.whitenton@nist.gov

ABSTRACT

This paper illustrates the errors due to integration time and size-of-source effects when measuring the temperature of segmented chip formation using infrared (IR) thermography. Segmented chip formation involves narrow periodic shear bands that experience rapid heating and move at high velocities and accelerations. As a result, the values of the measured temperatures depend strongly on the temporal and spatial measurement window used. In this study, an ideal infrared camera is simulated to understand the effects of integration time and size-of-source on the measurement. This analysis does not consider the temporal and spatial transfer functions of the camera system, thus simplifying the analysis to be applicable to all IR thermography users. Incorporating appropriate transfer functions would make the analysis specific to a given camera system. Finite element analysis (FEA) simulation results provide a reference cutting process which is manipulated to mimic motion blur and size-of-source effects. For this purpose, the FEA results adequately represent the cutting process with rapid heating and high chip velocities.

For the studied cases, size-of-source has relatively little impact on the measurement results when compared to the effects of integration time. Results show integration times from 1 μs to 90 μs significantly affect the measurement results. The maximum temperature measured by the simulated IR camera decreases from an FEA maximum of 735 °C to 668 °C at 90 μs integration time. Integration time significantly affects temperature measurement in the periodic shear band but does not significantly affect the simulated measurement error of the chip temperature near the tool rake face.

INTRODUCTION

Understanding the temperatures resulting from the metal cutting process leads to improvements in process efficiency. First, cutting temperature affects the dimensional accuracy and surface properties of the part and "adversely affects the strength, hardness, and wear resistance of the cutting tool" [1]. Tool coating and substrate materials, as well as cutting parameters such as rake, speed, and feed, can be optimized to reduce the temperatures and increase tool life. Second, models of the cutting process rely on temperature dependent material properties [2, 3]. Flow stress has been shown to decrease with increasing temperature. By understanding the temperatures experienced in metal cutting, material property tests can be performed at the appropriate temperatures and heating rates [4, 5]. Additionally, accurate measurements of metal cutting temperatures and forces provide benchmarks against which researchers in the modeling community can calibrate their models. Metal cutting models assist in the design of new tooling and the optimization of cutting processes.

Measurement error and uncertainty must be understood to properly interpret infrared (IR) thermography measurements of the metal cutting process [6, 7]. The dynamic character of segmented chip formation complicates temperature measurement [8, 9]. Specifically, the periodic shear band

[1] This paper is an official contribution of the National Institute of Standards and Technology and is not subject to copyright in the United States. Commercial equipment and materials are identified in order to adequately specify certain procedures. In no case does such identification imply recommendation or endorsement by the National Institute of Standards and Technology, nor does it imply that the materials or equipment are necessarily the best available for the purpose.

exhibits high thermal gradients in space and time, small feature sizes, and high accelerations and velocities. Consequently, the temperatures measured for these bands depend on the time duration and observation area of the measurement.

This study consists of a preliminary investigation into the effects of integration time and size-of-source on the measurement of segmented chips. Because there are numerous sources of uncertainty involved with such a measurement [9, 10], this study utilizes a simulation of an ideal IR camera to decouple measurement errors due to integration time and size-of-source from other sources of error. Process and camera parameters are based on the ongoing dual-spectrum high-speed microvideography research at the National Institute of Standards and Technology (NIST) [8, 9, 11-14]. Because the temperature field in an actual cutting process is not yet fully understood, results from a commercial finite element analysis (FEA) software package provide a known dynamic temperature field for the simulated IR camera to measure. The FEA results have been shown to adequately represent the periodicity of segmented chip formation [14].

INTEGRATION TIME

Integration time influences the measurable temperature range of the camera. Integration time refers to the time duration of each individual measurement the camera sensors make, commonly understood in photography as shutter speed. A longer integration time allows radiation from lower temperatures to be measured while the radiation from higher temperatures saturates the sensor signal. Conversely, a shorter integration time allows higher temperatures to be measured without saturating the signal, but does not allow the lower temperatures to be detected. This illustrates that integration time depends upon the desired temperature measurement range.

The range of measured wavelengths of light affects the achievable integration times. Most IR cameras measure a range of light wavelengths. To simplify the calculation of true temperature, a filter is typically used to limit the measurable light to a single wavelength. However, a single wavelength has less energy than a range of wavelengths at the same temperature. This requires the use of a longer integration time for the focal plane array (FPA) sensors to collect enough radiant energy to measure.

The desired measureable temperature range and different measurement methods cause large variations in integration time between studies. Therefore, the effect of integration time on the measurement error must be understood for researchers to properly express their results and for readers to be able to successfully compare results from different studies.

SIZE-OF-SOURCE

Size-of-source refers to the relative size of a feature in the image as compared to that of an individual sensor element area. Figure 1 illustrates the effects of size-of-source on temperature measurement. Figure 1(A) shows a sensor element area smaller than the feature area, allowing the sensor to measure the actual

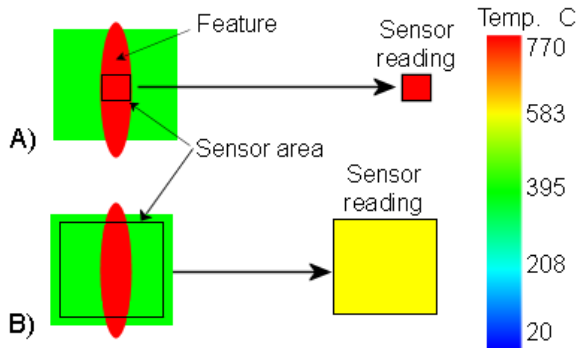

FIGURE 1. ILLUSTRATION OF THE SIZE-OF-SOURCE EFFECT. FOR A CONSTANT TARGET SIZE, A) SMALLER SENSOR ELEMENT AREA AND B) LARGER SENSOR ELEMENT AREA.

value of the feature. Figure 1(B) shows a sensor element area larger than the feature, resulting in the sensor having to integrate the area consisting of both feature and background values. This case results in a lower measurement value.

Camera magnification directly impacts size-of-source. Changing the magnification changes the apparent feature size, thus affecting the relative size between it and the sensor element area. Therefore, the effect of size-of-source must be understood to properly interpret the measurement results.

SIMULATION OF THE INFRARED CAMERA

This section discusses the method used for simulating an infrared camera measurement. It begins by explaining the infrared camera in the NIST dual-spectrum high-speed camera system. This camera provides a template for the simulation. Next, the FEA simulation used as the known temperature field for the IR camera simulation is described. Finally, the IR camera simulation methodology is presented. An ideal infrared camera is simulated to understand the effects of integration time and size-of-source on the measurement. This analysis does not consider the temporal and spatial transfer functions of the camera system, thus simplifying the analysis to be applicable to all IR thermography users.

NIST Infrared Camera

Current work at NIST uses a dual-spectrum high-speed camera system to observe and measure the cutting process. This camera system motivates the analysis presented in this paper. However, these results are illuminative for other camera systems as well. A brief overview of the camera system will be presented. Detailed information on the camera system and the accompanying work can be found in references [7, 8, 11-14].

The camera system images the side of an orthogonal cutting process. Cutting tests are performed at industrially relevant cutting conditions. The infrared camera in the dual-spectrum system obtains infrared images at 600 frames per second (fps). The camera bandwidth dictates that at the chosen frame rate, the camera uses an FPA 160 sensors wide and 120 sensors tall. The field of view is 0.96 mm wide and 0.72 mm

tall. Assuming 100 % coverage, each sensor element in the FPA observes an area of 35 μm^2; however, in reality FPAs have less than 100 % coverage, this results in a smaller sensor element size. A wavelength limiting filter is not used. By observing a large range of wavelengths (3.8 μm to 5.1 μm in this case), fast integration times can be used to minimize "motion blur."

Finite Element Analysis Simulation

The known dynamic temperature field for the IR camera simulation comes from a two dimensional turning simulation from Third Wave Systems' Advantedge software[1]. Prior work has shown that the simulation of AISI 1045 steel produces segmented chips with comparable segmentation periods to the experimental data [14].

The simulation parameters can be found in Table 1. These parameters produce a simulation output frame every 0.2 μs for the duration of one segment period (≈ 90 μs). This high sampling rate provides a fine temporal thermal field evolution of a single segment. Only one segment is needed because the simulation results do not exhibit significant randomness in the segmentation process. Figure 2 presents the resulting forces and maximum temperature of the simulation plotted against time. Vertical lines mark the beginning and end of the analyzed region. The individual node values of the FEA simulation are not evenly spaced and change due to velocity and dynamic re-meshing. Therefore, the thermal field results are exported as an audio video interleave (AVI) movie to provide a grid of equally spaced data points to be inserted into the IR camera simulation. The width (960 μm) and height (742 μm) of the movie frames approximately match the field of view of the NIST IR camera. The region with the most dynamic behavior was chosen.

TABLE 1. FEA SIMULATION PARAMETERS.

Workpiece	
Material:	AISI-1045 (200 Bhn)
Workpiece height (mm):	2
Workpiece length (mm):	10

Tool	
Material:	Carbide - General
Rake angle (°):	-7
Clearance angle (°):	7
Edge radius (μm):	20
Maximum tool element size (mm):	0.3
Minimum tool element size (mm):	0.03
Mesh grading:	0.4

Process parameters	
Feed (mm)	0.3
Depth of cut (mm)	1
Length of cut (mm)	3
Cutting speed (m/min)	250
Initial temperature (°C)	20

Simulation parameters: Results	
Number of output frames	15
Number of windows	1
Window start (mm)	1.579
Window finish (mm)	1.958

Simulation parameters: General	
Simulation mode:	Standard

Simulation parameters: Workpiece meshing	
Maximum number of nodes:	150000
Suggested maximum element size (mm):	0.2
Suggested minimum element size (mm):	0.01
Cutting edge radius to determine minimum element size:	0.8
Feed fraction to determine minimum element size:	0.1
Mesh refinement factor:	8 (fine)
Mesh coarsening factor:	4

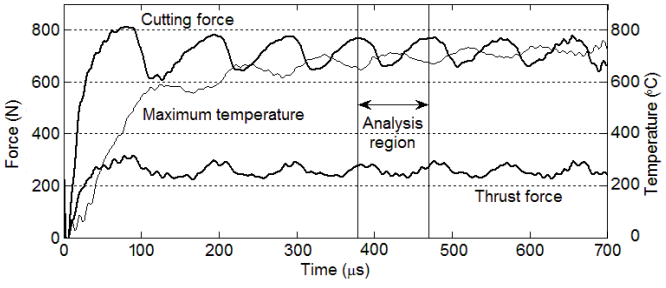

FIGURE 2. FEA SIMULATION RESULTS FOR FORCE AND MAXIMUM TEMPERATURE. VERTICAL LINES INDICATE THE BEGINNING AND END OF ANALYSIS REGION.

Camera Simulation Method

The analysis in this paper contains two sets of camera simulations: a set with constant sensor element size (matching the NIST camera system) and varying integration times, and a set with varying sensor element size and no consideration for integration time. Table 2 presents the parameters for both sets of simulations.

The first column of Table 2 presents the simulated integration times. Each integration time covers a certain number of AVI movie frames (n), shown in the second column. For example, a 1 μs integration time will last the duration of 5 AVI frames ($n = 5$), since the time between AVI frames is 0.2 μs. The third column presents the tensor size which refers to the total number of AVI movie pixels (p) used for the analysis of one simulated IR camera sensor element. The tensor is explained further in Figure 3.

The fourth and fifth columns in Table 2 present the simulated sensor areas used to investigate the size-of-source effects. The sixth column presents the corresponding tensor size for each analysis. The size-of-source simulation performed with a sensor element size of 35 μm^2 provides a point of comparison to the integration time simulations because all the integration time simulations are performed with a sensor element size of 35 μm^2. This comparison allows the effect of size-of-source to be differentiated from the effect of integration time.

Figure 3 presents a flow chart of the IR camera simulation process. For the chosen integration time, the analysis program reads n AVI movie frames created from the FEA simulation output. These n frames bracket the fully developed catastrophic

TABLE 2. IR SIMULATION PARAMETERS.

Integration time parameters			Size-of-source parameters		
Integration time	AVI movie frames (n)	Tensor size (p x p x n)	Sensor element area	AVI movie pixel area (p x p)	Tensor size (p x p x n)
1 μs	5	9 x 9 x 5	4 μm^2	3 x 3	3 x 3 x 1
10 μs	50	9 x 9 x 50	6 μm^2	6 x 6	6 x 6 x 1
25 μs	125	9 x 9 x 125	35 μm^2	9 x 9	9 x 9 x 1
45 μs	225	9 x 9 x 225	61 μm^2	12 x 12	12 x 12 x 1
60 μs	300	9 x 9 x 300	96 μm^2	15 x 15	15 x 15 x 1
75 μs	375	9 x 9 x 375	138 μm^2	18 x 18	18 x 18 x 1
90 μs	450	9 x 9 x 450	188 μm^2	21 x 21	21 x 21 x 1

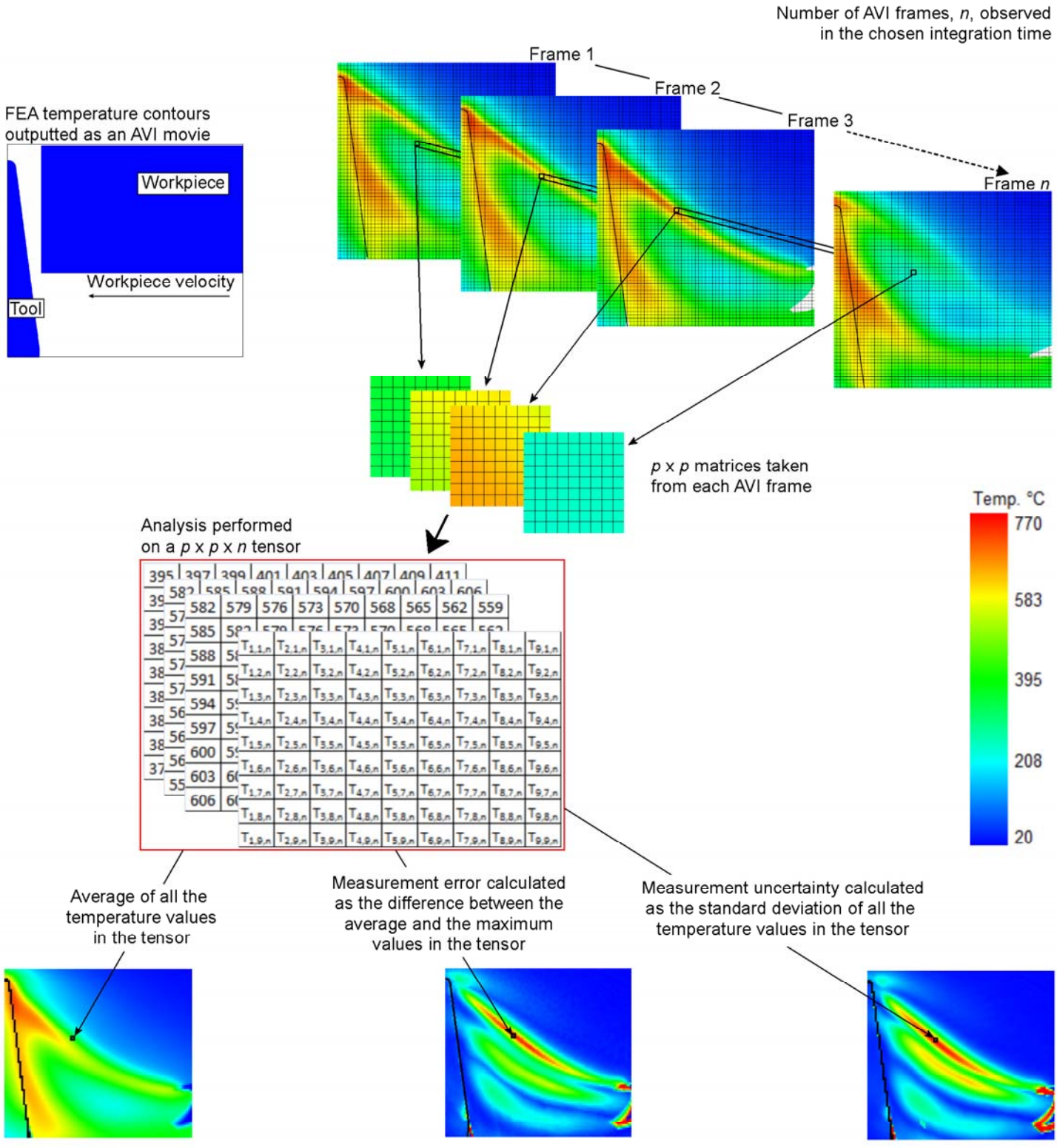

FIGURE 3. FLOWCHART DESCRIBING THE IR CAMERA SIMULATION METHOD. AN FEA SIMULATION PROVIDES THE EVOLUTION OF A KNOWN TEMPERATURE FIELD. AN AVI MOVIE OF THE TEMPERATURE FIELD HAS FRAMES SEPARATED IN TIME BY 0.2 μs. THE PROCESS IS REPEATED FOR EACH THERMAL CAMERA PIXEL.

shear band, where the temperature in the shear band is at a maximum. The pixels in the region of interest of each AVI movie frame are divided into groups of pixels where each group is a p x p matrix of pixels. A single group of pixels comprising a p x p x n tensor represents the temperature observed by a single sensor element in the FPA. Assuming a linear camera response, the measured temperature by a single sensor element is calculated using the average temperature value in the tensor. Repeating this process for each group of AVI pixels produces the simulated temperature reading of the IR camera.

In addition to calculating the average value of each tensor, the measurement error of local peak temperature and measurement uncertainty are calculated. The measurement error of local peak temperature is expressed as the difference between the maximum temperature value of the each tensor and the corresponding average temperature value because the peak temperature value is of interest when analyzing the periodic shear band. Measurement uncertainty is expressed as the standard deviation of the temperature values in each sensor element tensor.

RESULTS

Figure 4 presents the temperature field from the AVI movie; it also shows reference lines for the tool and the periodic shear band, as well as white cross-hairs which indicate the peak temperature location. Results from selected camera simulations are shown in Figure 9 through Figure 11 in the Appendix. In these figures, results for different integration times are compared to the values of the raw simulation output and the 35 μm^2 size-of-source simulation result. Figure 9 presents the simulated IR camera measured temperature field, Figure 10 presents the measurement error in local peak temperature, and Figure 11 presents the measurement uncertainty of each simulated IR camera pixel.

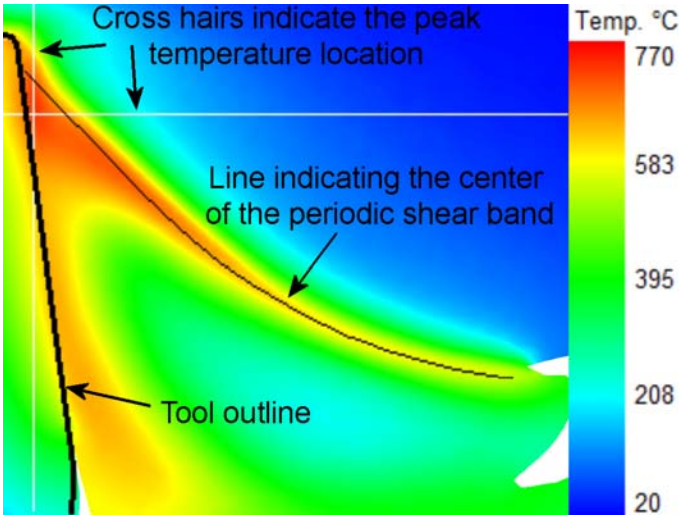

FIGURE 4. FEA SIMULATION TEMPERATURE FIELD OF THE FULLY DEVELOPED PERIODIC SHEAR BAND. TOOL OUTLINE, SHEAR BAND LINE, AND PEAK TEMPERATURE CROSS HAIRS ARE ALSO IN FIGURE 9 – FIGURE 11.

Peak Cutting Temperature

Peak cutting temperature is the maximum temperature experienced during the cutting process. In this analysis, the measured peak temperature is determined by the maximum simulated IR camera value. Figure 5 shows the effects of integration time and size-of-source on measured peak cutting temperature. The peak cutting temperature output by the FEA is 739 °C. An integration time of 90 µs, with a sensor size of 35 μm^2, produces a measurement error in peak temperature of -71 °C. Recall that the integration time simulations consist of a sensor element area of 35 μm^2. From the size-of-source analysis, a sensor observation area of 35 μm^2 produces a measurement error in peak temperature of -4 °C. These results illustrate that the integration time dominates the peak temperature measurement error for the integration time and size-of-source ranges investigated in this study.

The cross hairs in Figure 10 and Figure 11 show relatively low measurement errors and measurement uncertainties at the peak temperature locations. This occurs because the peak temperature locations reside along the rake face, which does not experience significant temperature oscillations. Similar results are experienced in the size-of-source results due to the

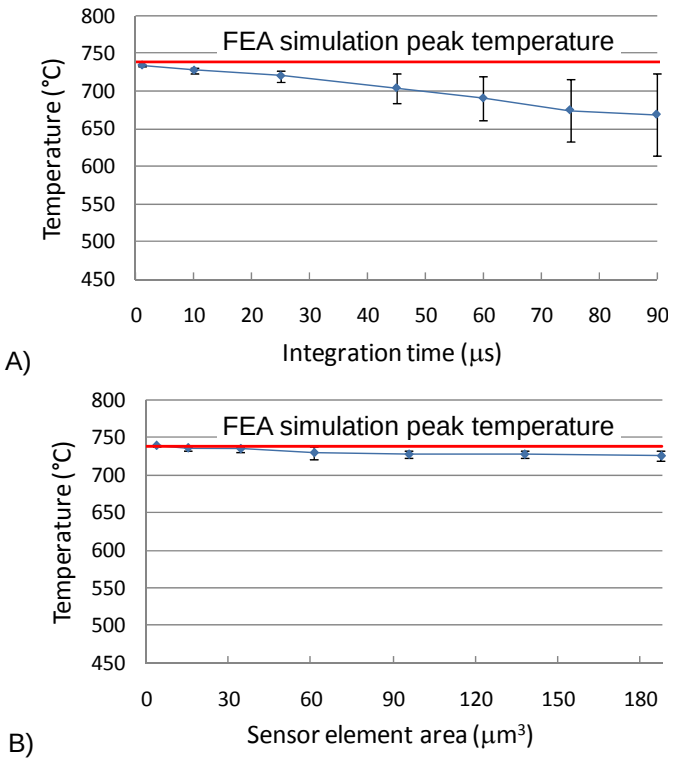

FIGURE 5. PEAK CUTTING TEMPERATURE VS. A) INTEGRATION TIME AND B) SENSOR ELEMENT AREA. ERROR BARS INDICATE THE MEASUREMENT UNCERTAINTY OF 1 STANDARD DEVIATION.

relatively less severe temperature gradient along the rake face when compared to the localized shear band.

Shear Band Temperature

The temperature of the periodic shear band is a more complicated measurement. First, the motion of the shear band makes the measurement highly dependent on integration time. A slower integration time exhibits more "motion blur" than a faster integration time. Secondly, in addition to motion, the periodic shear band experiences rapid heating. Finally, the heat flux from the rake face due to the tool-chip friction affects the temperature profile as the periodic shear band moves further along the tool rake face.

This final point makes determining the peak temperature of the periodic shear band difficult. To minimize the effects of the friction induced heat flux, the periodic shear band is assessed nearer to the free surface of the chip but far enough removed to avoid the "saw tooth" geometry on the free surface of the chip. For each integration time and size-of-source simulation result, the maximum temperature of a column of simulated IR camera pixels is used to find the peak temperature of the periodic shear band. At the same instant, the temperature profile in this column of values is compared to other integration and size-of-source results. To study the effect of different temperature profiles, two additional columns are chosen closer to the tool in the same frame as the original column. The temperature profiles of the periodic shear band closer to the tool exhibit less severe temperature gradients. This results from the friction heat flux rising the temperature of the surrounding material.

Figure 6 illustrates this analysis. The line labeled Column I on the temperature field in Figure 6(A) indicates the column of pixels used when detecting the maximum temperature of the periodic shear band. The other two lines indicate the other columns used to obtain temperature profiles. Figure 6(B) through Figure 6(D) present the temperature profiles of the columns of temperature data for each integration time.

Figure 7 extends the analysis presented in Figure 6. Instead of comparing the temperature profiles of the shear band, Figure 7 compares the peak shear band temperature located in Column I for each integration time and sensor observation area. The peak temperature in Column I of the FEA simulation is 567 °C. Error bars indicate the standard deviation of the temperature values in the corresponding tensors. In contrast to the peak cutting temperature measurement presented in Figure 5, where the 90 µs integration time produced a peak temperature measurement error of -71 °C, the 90 µs integration time causes a periodic shear band temperature measurement error of -194 °C. This difference is a result of measuring the small, rapidly moving shear band which experiences significant heating and cooling, while the location of the peak cutting temperature does not significantly move and experiences only minor fluctuations in temperature.

In contrast to the measurement error due to integration time, size-of-source produces drastically less significant measurement errors. A sensor size of 35 µm^2 results in a shear

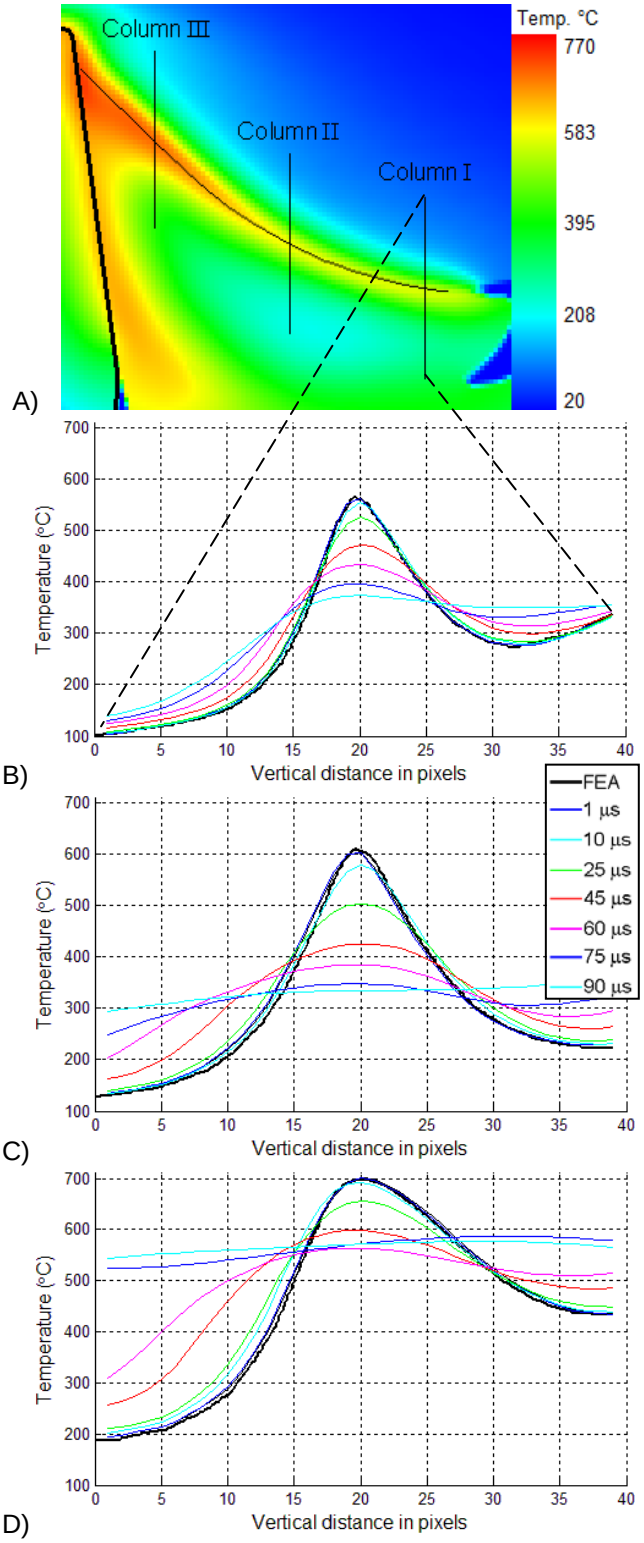

FIGURE 6. VERTICAL TEMPERATURE PROFILES OF THE PERIODIC SHEAR BAND TEMPERATURE FIELD. A) LOCATION OF EACH COLUMN, B) COLUMN I TEMPERATURE PROFILES, C) COLUMN II TEMPERATURE PROFILES, D) COLUMN III TEMPERATURE PROFILES.

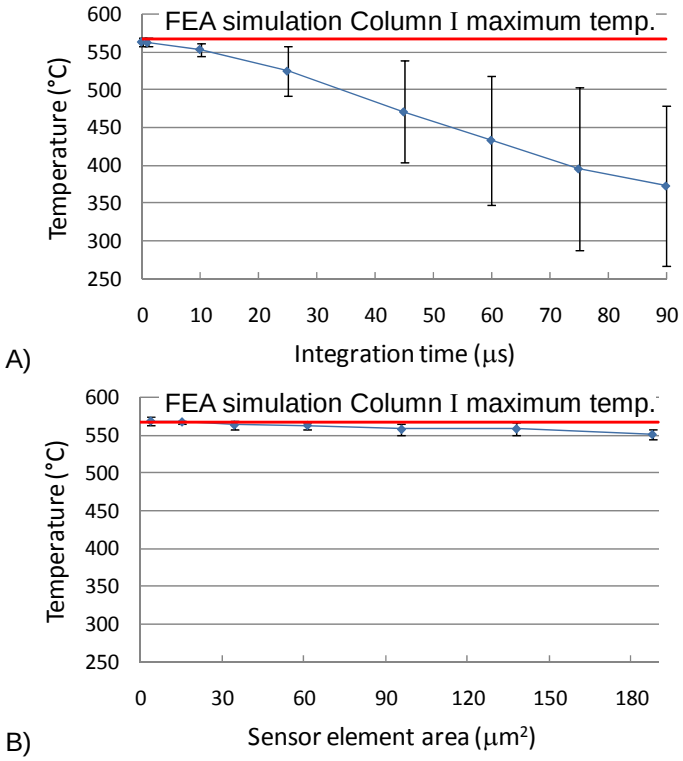

FIGURE 7. PERIODIC SHEAR BAND MAXIMUM TEMPERATURE IN COLUMN I COMPARED TO A) INTEGRATION TIME AND B) SENSOR ELEMENT AREA. ERROR BARS INDICATE THE MEASUREMENT UNCERTAINTY OF 1 STANDARD DEVIATION.

band temperature measurement error of -4 °C, and a sensor size of 188 μm^2 results in a shear band temperature measurement error of -16 °C. This shows that for the range of sensor element areas investigated in this study, the dynamic nature of the shear band has a greater impact on the measurement error than the relative size of the shear band.

Rake Face Temperature

Figure 10 and Figure 11 show a small measurement error and measurement uncertainty in the chip along the rake surface of the tool. This indicates the heat generated by friction produces a relatively stable temperature field compared to the temperature field further from the rake face, where the fluctuating temperature of the periodic shear band dominates.

DISCUSSION

This investigation only considered integration times up to and including 90 µs, which covers the chip segmentation period in this study. However, the cyclic behavior of the chip formation process allows the results at 90 µs to be applied to integration times that are significantly longer. This is illustrated in Figure 8 where the simulated IR camera sensor measurement and associated deviation reach steady state at values of 360 °C and 118 °C, respectively.

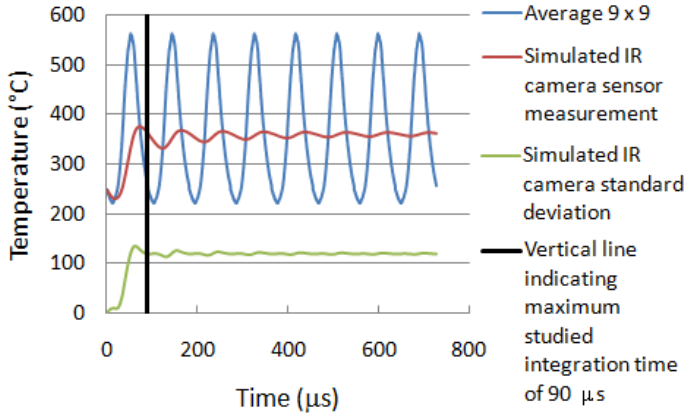

FIGURE 8. EXAMPLE SHOWING EFFECTS OF INCREASING INTEGRATION TIME. THE BLUE CURVE REPRESENTS THE AVERAGE TEMPERATURE OF A SINGLE 9 x 9 MATRIX DURING 725 µs OF THE CUTTING PROCESS. THE RED AND GREEN CURVES REPRESENT THE SIMULATED IR CAMERA MEASUREMENT AND STANDARD DEVIATION AT AN INTEGRATION TIME EQUAL TO THE CURVE'S POSITION ON THE X-AXIS.

Long integration times can be utilized when measuring the temperature distribution in the tool along the tool rake face, because the measurement error and measurement uncertainty along the tool are relatively low and appear less sensitive to increasing integration times. This could be advantageous when attempting to measure the heating due to friction between the tool and chip. In reality however, this region of the chip is more likely to reflect additional radiation from the tool rake surface and experience drastic changes in surface geometry due to the periodic side flow associated with segmented chips. Additional analysis is required to understand these effects on the temperature measurement, independent of integration time. However, care must be taken when measuring further away from the tool with long integration times since the measurement error and measurement uncertainty increase significantly, as shown in Figure 9(D), Figure 10(D), and Figure 11(D).

When studying the failure mechanism of the segmentation process, which is of particular interest in the machining of titanium alloys, a short integration time must be used to adequately capture the periodic shear band temperature. The results in Figure 6 show a significant difference in the temperature profile accuracy of simulations with integration times of 10 µs and 25 µs. This is further supported by the results shown in Figure 7.

Figure 10 and Figure 11 show an interesting behavior in the region surrounding the peak of the periodic shear band. Due to the rapidly increasing and decreasing temperature before and after the periodic shear band (supported in Figure 6), the measurement error on either side of the periodic shear band is greater than the measurement error at the center of the observed band. Therefore, the ability to precisely identify the location of

the catastrophic shear band significantly affects the measurement error.

Many error sources have not been addressed by this study [7]. Significant work is required to fully understand the measurement errors due to the process (emissivity, reflections, surface geometry, etc.), the optics (internal reflections, lens efficiency, etc.), and the FPA (sensor coverage, pixel cross-talk, non-linearity, etc.). Consequently, the analysis presented in this paper is a small part of a larger study required to fully understand the measurement errors associated with IR thermography of the metal cutting process.

CONCLUSION

This paper presented an analysis to characterize the measurement error and measurement uncertainty due to integration time and size-of-source when using IR thermography to measure segmented chip temperatures. Other sources of error and uncertainty were ignored in this study. The measurement error for the temperature of the periodic shear band exhibited substantial dependency on the integration time. A similar dependency was exhibited in the peak chip temperature measurement error and uncertainty, though to a lesser extent. Increasing integration time had minimal effect on the temperature field measurement error and uncertainty in the chip along the tool rake face. The peak temperature and shear band temperature measurement errors and uncertainties due to size-of-source effects were minimal for the chosen simulated range of sensor element areas.

These results indicate two outcomes. First, the dynamic nature of the shear band has a greater impact on the measurement error than the relative size of the shear band at the sensor element size range evaluated in this study. Therefore, variation in the camera magnification used within and between studies has a minimal impact on measurement error. However, at significantly larger sensor element size to target size ratios, measurement error due to size-of-source is expected to increase, especially when one considers a sensor element size which encapsulates the entire region of interest. Second, the measurement of the failure mechanism in the periodic shear band requires a camera with a short integration time. However, a camera with a longer integration time can be used when observing the peak cutting temperature and the temperature along the rake face. Despite these results, further work is required to fully understand all measurement errors associated with IR thermography of the metal cutting process.

ACKNOWLEDGMENTS

The authors would like to thank Robert Ivester, Johannes Soons, and Alkan Donmez of NIST for their support.

REFERENCES

[1] Kalpakjian, S., Schmid, S. R., (2003). "Manufacturing Processes for Engineering Materials, 4th Ed." *Pearson Education, Inc.*, Upper Saddle River, NJ.

[2] Johnson, G. R., Cook, W. H. (1983). "A Constitutive Model and Data for Metals Subjected to Large Strains, High Strain Rates and High Temperatures." *Seventh International Symposium on Ballistics*. April 19-21, The Netherlands.

[3] Marusich, T. D., Ortiz, M. (1995). "Modelling and Simulation of High-Speed Machining." *International Journal of Numerical Methods in Engineering*. 38(21), pp. 3675-3694.

[4] Jaspers, S. P. F. C., Dautzenberg, J. H. (2002). "Material behavior in conditions similar to metal cutting: flow stress in the primary shear zone." *Journal of Materials Processing Technology*. 122(2-3), pp. 322-330.

[5] Rhorer, R. L. (2003). "Dynamic Material Properties for Machining Simulation Using the NIST Pulse-Heated Kolsky Bar." *ASPE Proceedings*, October 26-31, Portland, Oregon.

[6] Davies, M. A., Ueda, T., M'Saoubi, R., Mullany, B., Cooke, A. L. (2007). "On the Measurement of Temperature in Material Removal Processes." *Annals of the CIRP*, 56(2), pp. 581-604.

[7] Whitenton, E., (2009). "Characterization of Uncertainties When Measuring Metal Cutting Temperatures Using Infrared Radiation Thermography." *Proceedings of SPIE*, 7299.

[8] Whitenton, E., Heigel, J., Ivester, R., (2008). "Measurement and Characterization of Dynamics in Machining Chip Segmentation." *Proceedings of the 11th CIRP Conference on Modeling of Machining Operations*, Gaithersburg, MD, pp.237-246.

[9] Heigel, J. C., Whitenton, E. P., (2009). "High-Speed Microvideography Observations of the Periodic Catastrophic Shear Event in Cutting AISI 1045 Steel." *Transactions of the North American Manufacturing Research Institution of SME*, 37.

[10] Holst, G. C., (2003). "Holst's Practical Guide to Electro-Optical Systems." *JCD Publishing*, Winter Park, FL.

[11] Ivester, R. W., Whitenton, E. P., (2003). "Simultaneous Visual and Infrared Imaging for Improved Machining Models." *NSJ Workshop on Research Needs in Thermal Aspects of Material Removal Processes*, pp. 70-76.

[12] Heigel, J. C., Ivester, R. W., Whitenton, E. P., (2008). "Cutting Temperature Measurements of Segmented Chips Using Dual-Spectrum High-Speed Microvideography." *Transactions of the North American Manufacturing Research Institution of SME*, 36, pp. 73-80.

[13] Whitenton, E., Ivester, R., Yoon, H., (2005). "Simultaneous Visible and Thermal Imaging of Metals During Machining." *Proceedings of SPIE*, 5782, pp. 71-82.

[14] Ivester, R. W., Whitenton, E. P., Heigel, J. C., Marusich, T., Arthur, C., (2007). "Measuring Chip Segmentation by High-Speed Microvideography and Comparison to Finite-Element Modeling Simulations." *Proceedings of the 10th CIRP International Workshop on Modeling of Machining Operations*, Calabria, Italy, pp. 37-44.

APPENDIX

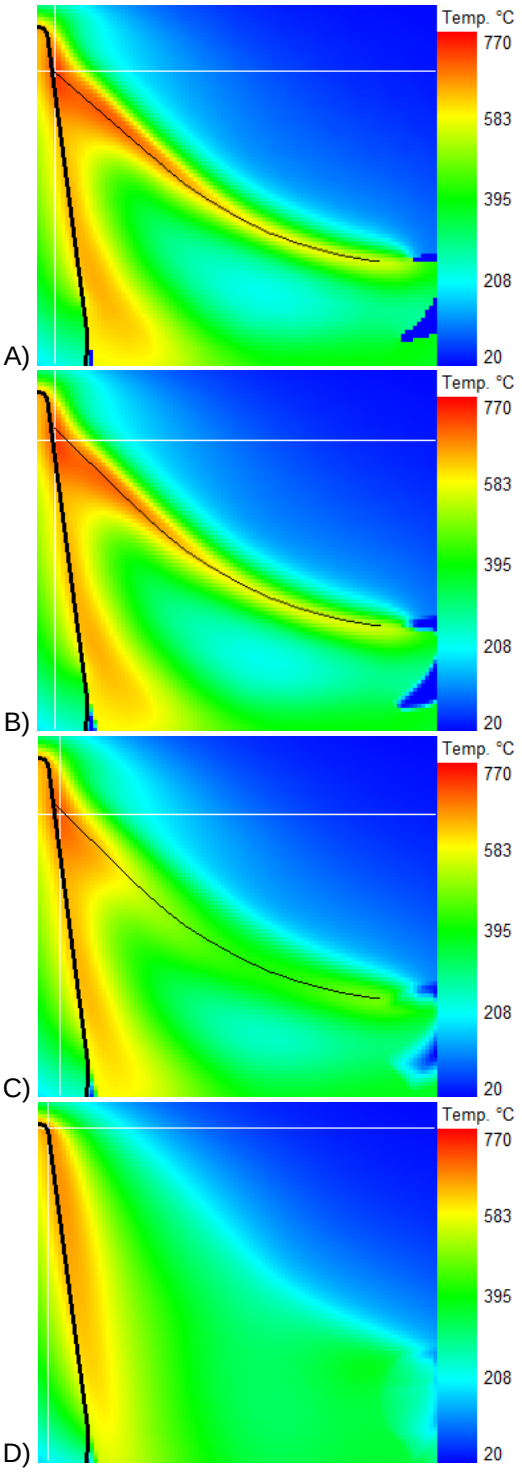

FIGURE 9. SIMULATED IR CAMERA MEASUREMENT RESULTING FROM THE AVERAGE TEMPERATURE VALUE OF EACH 9 x 9 x n TENSOR. A) 35 μm^2 SIZE-OF-SOURCE (9 x 9 x 1), B) 10 μs INTEGRATION TIME (9 x 9 x 50), C) 45 μs INTEGRATION TIME (9 x 9 x 225), AND D) 90 μs INTEGRATION TIME (9 x 9 x 450).

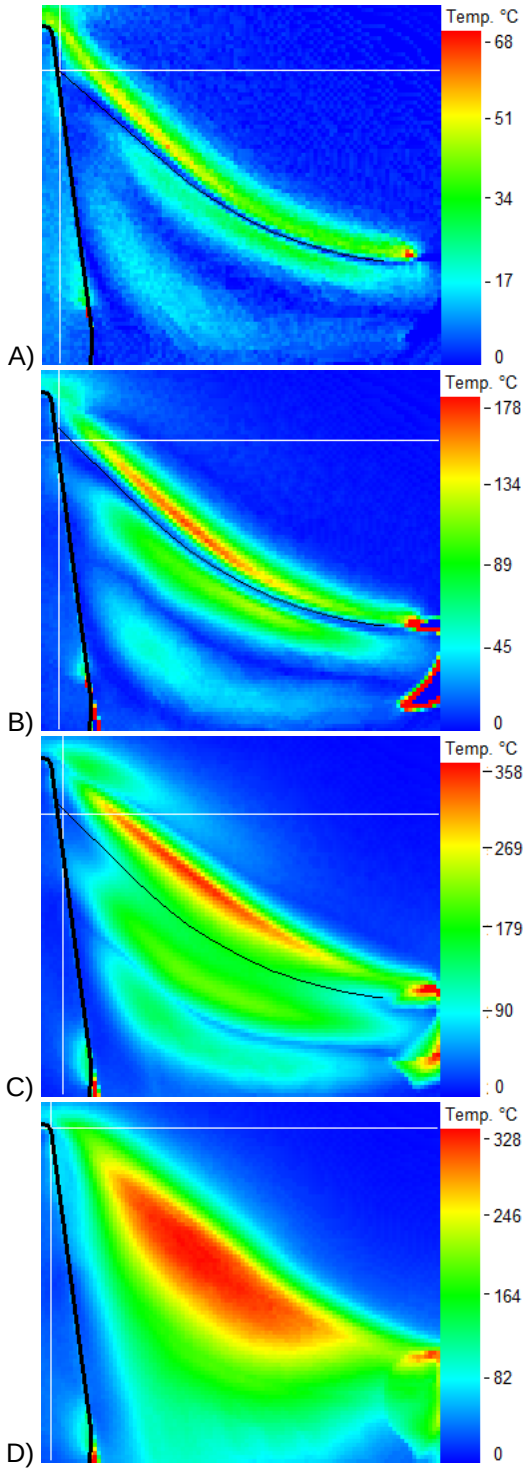

FIGURE 10. SIMULATED IR CAMERA MEASUREMENT ERROR RESULTING FROM THE DIFFERENCE BETWEEN THE AVERAGE AND MAXIMUM TEMPERATURE VALUES OF EACH 9 x 9 x n TENSOR. A) 35 μm^2 SIZE-OF-SOURCE (9 x 9 x 1), B) 10 μs INTEGRATION TIME (9 x 9 x 50), C) 45 μs INTEGRATION TIME (9 x 9 x 225), AND D) 90 μs INTEGRATION TIME (9 x 9 x 450).

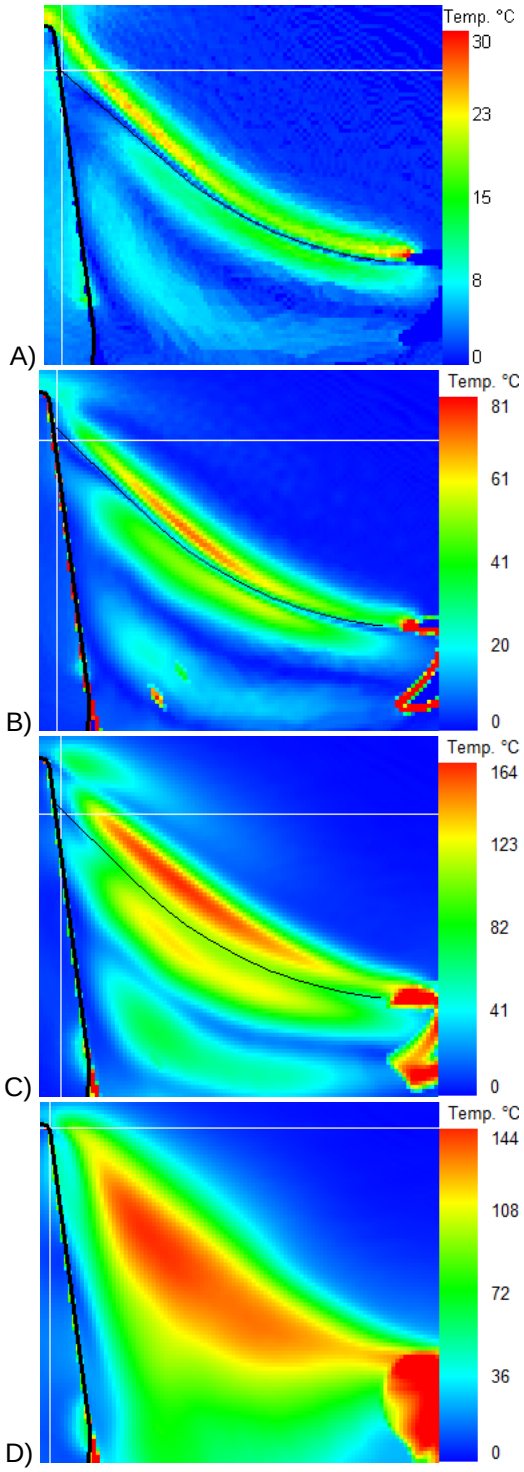

FIGURE 11. SIMULATED IR CAMERA MEASUREMENT UNCERTAINTY RESULTING FROM THE STANDARD DEVIATION OF THE TEMPEARTURE VALUES OF EACH 9 x 9 x n TENSOR. A) 35 μm^2 SIZE-OF-SOURCE (9 x 9 x 1), B) 10 μs INTEGRATION TIME (9 x 9 x 50), C) 45 μs INTEGRATION TIME (9 x 9 x 225), AND D) 90 μs INTEGRATION TIME (9 x 9 x 450).